Journal of River Engineering
Volume 2, Issue 9, 2014
http://www.scijour.com/jre
SCIJOUR

Observations and Modeling of Transverse Mixing in a Natural Gravel-Bed River

William Swick[1,*], Jamie MacMahan[2], Ad Reniers[3], Ed Thornton[2]

[1]Oceanography Department United States Naval Academy, Annapolis, MD 21402
[2]Oceanography Department, Naval Postgraduate School, Monterey, CA 93933
[3]Applied Marine Physics, University of Miami, Miami, FL 33149

ABSTRACT

A comprehensive, continuous, point-source, dye concentration experiment was performed on the Kootenai River, Idaho, USA to describe natural river transport and mixing dynamics. Centerline fluorescent dye concentration releases formed quasi-steady state plumes. Combinations of stationary and moving observational platforms were used to describe the dye concentration plume spreading and the velocity field throughout a 550 m study reach.Observational platforms included 13 fluorescent concentration sensors, 5 acoustic Doppler profiling current meters and one acoustic Doppler velocimeter. Natural channel transverse diffusivities are calculated using concentration measurements. Observed mixing is strongly controlled and dependent on channel features. Field observations are used to initialize and validate an open source, processed-based, three-dimensional (3D) hydrodynamic model (Delft3D-FLOW). Model simulations show good agreement with the in situ measurements with velocity fields (velocity magnitude R^2=0.87), water levels (R^2=0.97) and concentration spread. To examine the mixing processes, prominent bathymetric features of a constriction, riffle and embayment are isolated and idealized. The numerical investigations emphasize that linear superposition of channel feature concentration spread effects does not provide accurate overall spreading estimates. Accurate concentration spreading prediction required resolving complex coupled secondary velocity fields controlled by bathymetric variability at all scales. These coherent velocity structures are responsible for the observed spatial concentration distributions, which are shown to spatially enhance and restrict lateral transport, resulting in a strongly non-linear mixing response.

KEYWORD

Dispersion, Delft3D, Lateral, Mixing, Dye, Concentration

INTRODUCTION

The ability to predict the flow dynamics of a natural river enables water quality managers to better plan for and mitigate environmental impacts. The understanding of flow dynamics applied to known urban discharges allows for better monitoring and planning controls to ensure environmental and human well-being. For example, environmental planners can apply river dynamics knowledge to help promote the transport of larvae from spawning to rearing habitats. On shorter time scales, detailed flow dynamics can used to assess the immediate impact, and direct required actions, to advert the potentially damaging effects on the environment and human health due to unintentional spills. Numerical models have been compared successfully with hydraulically and geometrically controlled laboratory experiments [1-5]. However, laboratory settings remove aspects of the natural bathymetric variability and subsequently underestimate natural channel mixing. Previous researchers have shown natural bathymetry irregularities have a large effect on mixing [6,7]. Transport, dispersal and convergence properties of a natural river are governed by large-scale motions controlled by channel geometric variability. These processes,coupled with the smaller scale diffusion processes, result in mixing, which cannot be estimated with simple models using average hydraulic and geometric channel parameters alone. For example, transverse spreading rates (diffusivity, k_n) in natural channels without curvature and with relatively constant depth and width profiles are a factor of two larger than measured in the laboratory [6,8]. There are few field observations of dye concentration transport in natural river flow with sufficient spatiotemporal resolution to allow for comparison to a numerical model. Dow et al [7]. only used bathymetric and velocity observations to calibrate a 2D hydrodynamic model to evaluate transverse mixing characteristics of a wastewater treatment plant. Constantinescu et al [9] .

*Corresponding Author: William Swick
E-mail:
Telephone Number: Fax. Number:

Journal of River Engineering
Volume 2, Issue 9, 2014
http://www.scijour.com/jre
SCIJOUR

used concentration visualizations of a mixing experiment in a natural channel with a groin field and found qualitative agreement with a detailed large-eddy-simulation (LES) numerical investigation. More comprehensive field experiments are needed to directly investigate the complexities of natural channel mixing and to further validate 3D numerical transport and mixing models.

In this study, comprehensive field observations of dye concentration transport and mixing obtained on the Kootenai River in August 2010 are compared with results of 3D Reynold's Averaged Navier-Stokes (RANS) process modeling with Delft3D-FLOW. The dispersion experiment was performed using Acoustic Doppler Current Profilers (ADCPs) for current profile measurements, an Acoustic Doppler Velocimeter (ADV) for turbulence measurements, and a combination of Lagrangian and Eulerian platforms equipped with dye sensors to capture the evolution of the dye concentration plume. Bathymetric surveys, in situ water elevations, and stream discharge are inputs for the model boundary conditions. The numerical flow field is compared to velocity profiles obtained throughout the study area. After successful model validation, the effects of river geometry on transport and mixing processes are numerically investigated by decomposing the natural river features into idealized cases accounting for a constriction, riffle and embayment. The lateral momentum fluxes associated with these features are computed and compared with modeled concentration behavior and experimental observations.

FIELD EXPERIMENT

A small, 30 m wide and 550 m long channel, was selected based on existing U.S. Geological Survey (USGS) stream channel bathymetry and substrate data [10-12]. The channel is considered straight with a sinuosity of 1.01, defined as path distance divided by straight-line distance, and shallow with an average thalweg depth of 1.6 m and mean depth of 0.7 m. The channel bathymetry is transformed to a river local coordinate frame by the method outlined in Legleiter and Kyriadkidis [13], where the streamwise axis, *s*, is along the river centerline (positive in the downstream orientation), and the transverse axis, *n*, is normal to the river centerline (positive to the left) (Fig.1).

The channel contains a constriction and riffle located at s=160 to 223 m, where *s*=0 m is the location of the dye release, and a natural embayment at *s*=247 to 355 m (Figure 1). The bottom consists of poorly sorted cobble and gravel. Measured particle-size at a cross-section 5 km upstream of the study site ranged from 21 to 78 mm (D16 and D84), with a median particle-size (D50) of 40 mm (Fosness and Williams, 2009). Discharge is controlled 100 km upstream at the Libby Dam and was constant throughout the experiment.

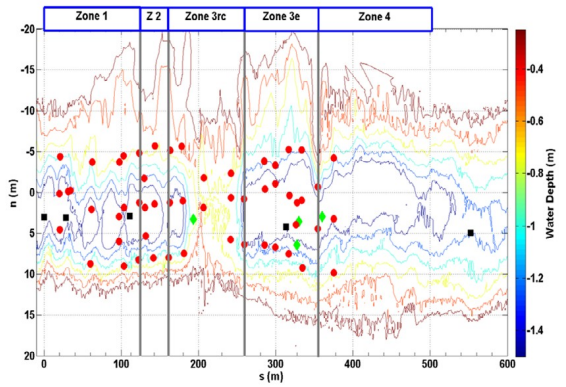

Fig.1. Plan view of the Kootenai River Study reach, ID, U.S.A. in a local coordinate frame. Depth contours are plotted as color lines with color scale plotted to the right. Black squares indicate vertical fluorometer array location, green diamonds are ADV frame locations and the red circles are ADCP locations.

Additional bathymetric surveys were performed to supplement the USGS bathymetry and to ensure that the river morphology had not evolved. A survey-grade GPS and 200 kHz echo sounder were mounted on a motorized electric kayak. The kayak traversed the channel with streamwise transect spacing of ~10 m. Channel bank locations and water elevations were obtained from a survey-grade GPS mounted on a person walking the water line. Vertical and horizontal control for the river survey is based on the previously established USGS control stations [10]. The hydraulic conditions were monitored using a surveyed pressure sensor located 500 m upstream of the concentration release point. Discharge was measured by repeated transectsusing a 600 kHz ADCP. Both the water elevation and channel discharge (9.7 m^3/s) were constant for the duration of the study.

Prior to the concentration release, 20-minute time-averaged velocity profiles were acquired at 47 locations throughout the channel using downward-facing 2 MHz ADCPs mounted on three catamarans sampling at 1 Hz with 0.05 m surface blanking distance and 0.20 m bin size (Fig.1). Mean velocities ($\bar{u}$) are 0.5 m/s in the channel center and 0.3 m/s near the channel banks, which is typical of open channel flow regulated by channel depth variations. Near the riffle/constriction, *s*=160 m to 223 m, the channel narrows from 30 m to 15 m and shallows from 1.6 m to 0.7 m causing the flow to increase to a maximum speed of 1.4 m/s. Vertical velocity profiles showed good agreement (R^2~0.7) with a logarithmic law of the wall profile in the center of the channel, where R^2 is the log-linear regression coefficient squared. ADCP velocities are inherently noisy and require approximately 3 minutes of averaging to reduce the noise [14]. Therefore, a faster-sampling (32Hz), single-point ADV was used to resolve smaller scale flow fluctuations at different locations in the channel. The ADV was mounted on a fixed frame at a height of 1 m off the river bed (approximate mid-water column) and was deployed for approximately 1.5 hours at four locations, *s*=194 m, 327 m, 330 m and 360 m (Fig.1).

Journal of River Engineering
Volume 2, Issue 9, 2014
http://www.scijour.com/jre
SCIJOUR

Two dye concentration studies (T1 and T2) were conducted on August 16. Rhodamine-WT dye concentrate (2.5% by weight) was released continuously at 6 mL/s from an 18.9L container onboard a kayak fixed at the channel centerline. The fluorescent dye was released for approximately one hour through an 8 mm diameter tube located 0.05 m below the waterline through a butterfly valve that was manually controlled to provide a constant discharge. Dye concentrations, *C* (ppb), were acquired with 13 fluorometers that sampled at 0.9 Hz with a Rhodamine detection range of 0 to 234 ppb and a sensitivity of 0.09 ppb. It is assumed there was no concentration decay with time owing to the short duration of the each dye release (one-hour) compared to the photo degradation of five to seven days for the Rhodamine-WT dye used [15]. Temporal and spatial dye concentrations were measured using fluorometers collocated with GPS units mounted on fixed and moving platforms. The GPS units, sampling at 0.5 Hz, provided absolute post-processed positions with accuracies <0.4 m [13]. The temporal evolution of the dye concentration plume was acquired by deploying a total of 10 fluorometers at streamwise distances *s*=0m, 28m, 110m, 313m, and 550m in the channel centerline (Fig.1). At 0m, one fluorometer was deployed at the surface. At 28m and 110m, three fluorometers were deployed at the bottom, mid-depth, and surface. At 313m, two fluorometers were deployed at bottom and the surface. At 550m, a single fluorometer was deployed at the surface. Assuming stationarity, the surface spatial distribution of the dye concentration plume was mapped utilizing three, 1m long, mobile catamarans each equipped with a GPS and fluorometer. Concentration sampling did not commence until steady state conditions were established, which was determined *a priori* to be 25 minutes after dye was released. The sampling delay time of 25 minutes (925 s) was based on time for the dye to travel to the farthest downstream sampling point, 550m, multiplied by 1.5 to account for the largest scale temporal fluctuations of the velocity field based on channel parameters, mean velocity and width [7]. Dye concentration cross-shore transects were obtained by personnel located on opposite channel banks slowly pulling two lines attached to each catamaran. The slow pull across the 30 m wide channel took approximately 2.5 minutes to complete. To minimize flow disturbances, care was taken to keep the lines out of the water. Following each completed transect the catamaran was relocated approximately 8 m downstream and the sampling repeated. The transverse concentration profiles were acquired using three catamarans simultaneously between *s*=28 m to 550 m requiring approximately 35 minutes, which resulted in 66 and 70 individual concentration profiles for the first and second concentration release respectively. Surface dye concentrations transect locations for each release are superimposed on channel bathymetry (Fig.2a and b).

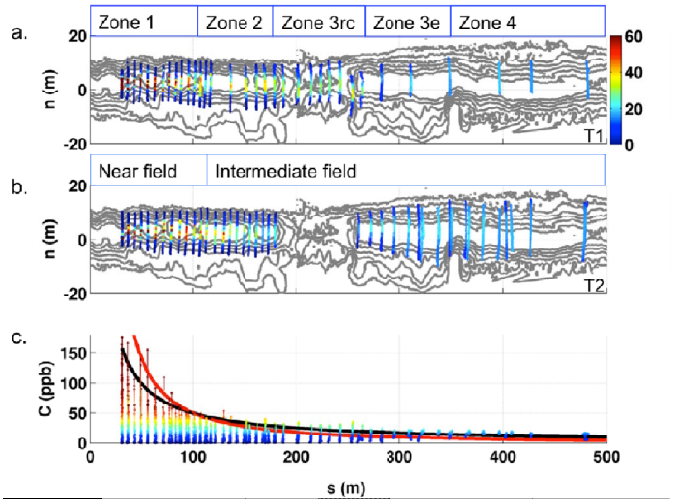

Fig.2. Plan view of surface dye concentration transects, C(n,s), (color dots, scale in ppb on right) overlaid on river bathymetry (gray lines) for a) T1 and b) T2. c) Concentration decay 3D mixing behavior ($C_{max}(s)\sim s^{-3/2}$) (red Line) and 2D mixing behavior ($C_{max}(s)\sim s^{-1}$) (black line). Four zones along the channel based on plume mixing behavior and channel geometry are labeled at the top. At the first zone, 0<s<125 m, the plume is mixing in three-dimensions. At the second zone, 125<s<160 m, complete vertical mixing has occurred. The third zone, 160<s<350m, contains channel bathymetry and geometry features. Subsets to zone 3 are riffle/constriction location, 160<s<260 m, Zone 3rc, and the embayment, 260<s<350 m, Zone 3e. The fourth zone, s>350 m, is downstream of channel features where concentrations are well mixed.

Concentration transport, *M(s)* (ppb m^3/s),

$$M(s) = \int_0^B h(n,s)\bar{V}(s)C(n,s)\,dn, \qquad (1)$$

is calculated to ensure that the sampling methods adequately captured the concentration plume, where *h(n,s)* is the depth of point measurements at river coordinate (n,s), $\bar{V}(s) = Q/A(s)$ is the mean streamwise velocity, *Q*is a constant discharge, *A(s)* is cross sectional area at each streamwise location, and *B* is the transect width. Assuming the concentration is well-mixed over the vertical and there is negligible concentration trapping, the transect sampling is complete when *M(s)* is constant downstream. Therefore the T1 and T2 *M(s)* releases should have similar mean concentration transport values with only small fluctuations over the length of the reach. Measured T1 and T2 *M(s)* have similar mean values of 120 and 122 ppb m^3/sbut large fluctuation downstream, standard deviations of 29% and 23% respectively. Closing the transport values in natural settings tends to be problematic [17,18]. These transport results improve previous concentration studies in natural environments and the mean and variability of the transport measurement were consistent between deployments.

Transverse dispersion,$\sigma_n^2(s)$, is determined by calculating the 2nd moment of *C(n,s)* defined as:

$$\sigma_n^2(s) = \frac{\int_0^B |n(s)-\mu(s)|^2 C(n,s)dn}{\int_0^B C(n,s)dn}, \qquad (2)$$

where$\mu(s)$ is the 1st moment of *C(n,s)*defined as,

$$\mu(s) = \frac{\int_0^B nC(n,s)dn}{\int_0^B C(n,s)dn}. \qquad (3)$$

Transverse diffusivity, k_n, is determined by,

Journal of River Engineering
Volume 2, Issue 9, 2014
http://www.scijour.com/jre
SCIJOUR

$$k_n = \frac{\bar{V}}{2}\frac{d\sigma_n^2}{ds}, \qquad (4)$$

where $\bar{V}(s)$ is used to transform time to space. The transverse profile-integrated statistics, (2) and (3), are averaged over all transects within streamwise distances of 2 m to collapse repeated transects values. Averaging the statistics, as opposed to the transects themselves, preserves the individual transect center of mass. This method avoids potential meander biases in the dispersion, which would otherwise blur the profile [18]. The total number of downstream transect locations is thereby reduced from 66 and 70 to 41 and 50 for T1 and T2.

CHANNEL FEATURES AND OBSERVATIONS

The experiment measurements and subsequent analysis are divided into four zones, based on plume evolution from the source and channel geometry (Fig.2). In Zone 1 (0 m<s<125 m), the plume is mixing in three dimensions (s, n, and vertical, z). Zone 2 (125 m<s<160 m) begins once complete vertical mixing has occurred. In Zones 1 and 2, the channel is relatively straight and depth and width are relatively constant (Fig.2a). Zone 3 (160 m<s<355 m) is a section characterized by large bank and bathymetric irregularities that modify the flow and corresponding dispersion. This zone is subdivided to emphasize transport and mixing effects between distinct flow regimes induced by the irregular channel features. The first feature is a riffle and constriction (Fig.2a Zone 3rc) located 160 m<s<260 m. In Zone 3rc, the channel contracts (25 m to 15 m) and shallows (1.7 to 0.7 m). The second feature is an embayment (Fig.2a Zone 3e) located 260<s<355 m. In Zone 3e, the channel widens (15 m to 30 m) and rapidly deepens from 0.7 m to 1.7 m. The final section, Zone 4, begins downstream of the Zone 3e at 355 m<s<550 m. Within Zone 4, the channel geometry returns to being relatively straight with small depth and width irregularities.

In Zone 1, the constant source surface plume exhibits narrow filaments of high and low concentration streaks. The surface, mid-depth and bottom concentration time series, at 28 m and 110 m (not shown), depict sawtooth structures typical of smaller scale diffusive processes superimposed on the larger scale coherent advective motions (Holzer and Siggia, 1994). The decay of the concentration maxima, $C_{max}(s)$, with downstream distance is in good agreement (R^2=0.86, 0.84 for T1, T2) with a 3D mixing behavior, $C_{max}(s) \sim s^{-3/2}$(Fig.2c -red line) [8]. The transverse concentration distributions, $C(s)$, values are peaky (kurtosis>3) and skewed towards river-left (positive skewness) compared to a Gaussian distribution with skewness equal to 0 and kurtosis equal to 3 (Table.1). Dispersion is small and constant (k_n=0.02, 0.01 m^2/s) and spreading is linear in time (R^2 = 0.80, 0.87) (Fig.3). Measured Zone 1 $k_n$is in close agreement with reported transverse dispersion measurements in a straight natural channel with similar depth, width and discharge parameters [19].

In Zone 2, $C_{max}(s)$ continues to decay with downstream distance exhibiting a 2D mixing behavior, $C_{max}(s) \sim s^{-1}$, (R^2 =0.82, 0.82 for T1, T2) (Fig.2 c (black line)) indicating the plume has completely mixed in the vertical [8]. The ratio of the river-bed concentration to the surface concentration can also be used to determine the extent of vertical mixing [6]. When river-bed concentration to the surface concentration is close to one, the concentration is considered vertically well mixed. Interpolating the average concentration ratios of bed and surface at s=28 m, 110 m and 313 m, (not shown), the distance of complete vertical mixing is found to occur slightly downstream of s=110 m, whichsupports the observed decay behavior of $C_{max}(s) \sim s^{-1}$. Within Zone 2 the concentration plume transverse distribution becomes symmetrical, with $C(s)$skewness values decreasing to zero at s=140 m, with slightly flatter (kurtosis<3) than a true Gaussian shape (Table.1). The transverse diffusionk_n, (0.01, 0.02 m^2/s) remains small and approximately constant (Table.1, Fig.3). The constant k_n, value throughout Zone 1 and 2 indicates the plume is not yet influenced by bathymetry induced secondary circulations. Weak secondary circulations would increase mixing by a factor of two and strong mixing interfaces could result in $k_n$values 30 times larger than the typical (observe) Zone 1 and Zone 2 values [6].

Table 1.Zonal average C(s) statistics for T1 and T2.

	Zone 1	Zone 2	Zone 3rc	Zone 3e	Zone 4
Skewness	1.50, 1.75	0.70, 0.53	0.17, 0.18	-0.21, 0.17	-0.50, -0.64
Kurtosis	4.94, 6.83	2.26, 2.05	1.62, 1.64	3.10, 1.94	2.25, 3.05
k_n (m^2/s)	0.02, 0.01	0.01, 0.02	0.01, NA	0.01, 0.06	0.02, 0.01

In Zone 3rc, the dispersion remains small and constant (k_n=0.01 m^2/s for T1, sampling was sparse for T2 in Zone 3rc). Downstream at the transition between Zone 3rc and 3e, a strong mixing interface is present due to the jet-like flow in the center of the channel and stagnant water near the banks. The mixing interface has a large influence on mixing. The concentration plume shifts towards the slower water within the embayment on river-right, which alters the previously symmetrical $C(s)$ in Zone 2 and Zone 3rc to negatively skewed distribution in Zone 3e for T1 (Table.1). For release T2, σ_n^2increases by a factor of six (k_n=0.06m^2/s) [Figure 3, red dots t>500s] linearly in time (R^2=0.82). Release T1 σ_n^2 spread is slow (k_n=0.01 m^2/s) with the behavior nonlinear and noisy (R^2 =0.15), so a regression line for σ_n^2 is not included (Fig.3, black dots t>500s). The T2 $k_n$increase between Zone 3rc and 3e fits within the expected range 2 to 30 based on published data from transverse dispersion measurements [6].

The T1 and T2 difference within Zone 3e are due to the physical sampling width differences between the two concentration releases (Fig.2a and b). Downstream of the release point, T1 under-sampled the plume width extent, which resulted in smaller perceived T1 σ_n^2 values. The T1 and T2 sampling width differences are accounted for by normalizing σ_n^2 by the variance of a uniform distribution over the respective sampled width. The normalization,$\sigma_n^2(s)/\sigma_{uniform}^2(s)$, accounts for the sampled

Journal of River Engineering
Volume 2, Issue 9, 2014
http://www.scijour.com/jre
SCIJOUR

width and allows concentration dispersion to be defined relative to the channel. The normalized spreading calculation provides values of 0 for no mixing and 1 for complete transverse mixing (Fig.4). Normalized spread, $\sigma_n^2(s)/\sigma_{uniform}^2(s)$, aligns T1 and T2 measurements, while preserving the observed spreading behavior (Fig.4).

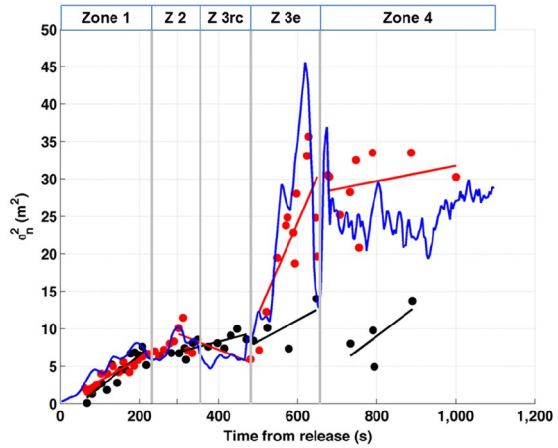

Figure 3. Transverse spreading, σ_n^2, in time calculated for T1 and T2 (black and red dots respectively). Initial constant mixing in the near and intermediate fields is shown with the linear regression fits (solid lines). Pre-riffle k_n= 0.01 m^2/s and 0.013 m^2/s with R^2 = 0.92 and 0.93 for T1 and T2 respectively. Post-riffle k_n= 0.06 m^2/s with R^2 = 0.82 for T2 before complete mixing at t~650s. Delft3D calculated transverse dye dispersion (blue line). Gray lines indicate spatial zones.

In Zone 4, transverse dispersion asymptotes and reaches a value of 35 m^2, indicating uniformly mixed when normalized by sample width (Fig.4). C(s>355 m) are nearly uniform with a standard deviation of 1 ppb for T1 and 3 ppb for T2. The kurtosis is close to 3 but the negative skewness in the plume distribution remains in Zone 4 (Table.1). The mechanisms responsible for the observed river-right asymmetry are investigated by examining the transport effects due to persistent flow structures induced by the channel features in section 4.3.

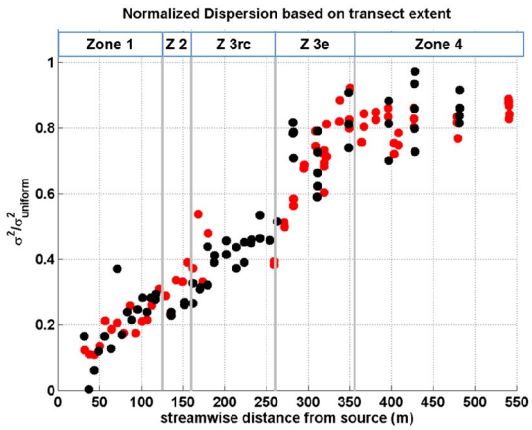

Fig.4. Normalized transverse mixing verse streamwise distance. Tracer studies T1 (black circles) and T2 (red circles). Leveling for both releases occurs at s=350 m as the concentration plume becomes bounded by the channel.

ANALYSIS

The concentration observations suggest k_n is highly variable in the vicinity of channel irregularities (Table.1). The effects of channel geometry on mixing are investigated by scaling the observed velocity spectra by predominate channel length scales of depth and width. The resultant concentration spectra are then examined in the context of the underlying flow dynamics. Velocity and concentration spectra are calculated using a 7.5 min Hanning window with 50% overlap for 90-min records of ADV velocities (Figure 1, green diamonds) and 30-min records of fluorometer concentrations (Figure 1a black squares) resulting in a frequency resolution of 0.002 Hz and 24 and 8 degrees of freedom respectively. The ADV velocity spectral components, u_s,u_n, w, at all locations converge towards isotropic motion at higher frequencies (f >~0.3 Hz) (Figure 5), which scales with channel dimensions $f \approx U/h$, where U is the mean velocity [20]. At f >0.3 Hz, it is expected that all velocity components would decrease at the same rate. However, the horizontal noise due to the frame motion is evident in the ADV data at f >1 Hz. At frequencies lower than $f \approx U/h$, the flow is anisotropic where the horizontal fluctuations become one to two orders of magnitude larger than vertical scales. Additionally,there are significant differences in the transverse velocity components at different streamwise locations. ADV locations immediately downstream of the riffle at s=327 and 330m (Fig.5 blue and black lines) contain one order of magnitude more transverse energy in the lower frequencies than ADV locations upstream (s=195m) and farther downstream (s=361m) from the riffle, which fits the river dimensional scaling $f \approx U/B$ ~0.02 Hz, where B is the channel width.

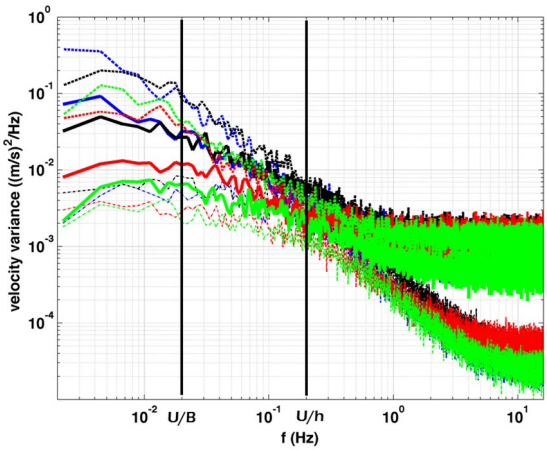

Fig.5. ADV velocity spectra for the stream velocity (dashed lines), transverse velocity (solid lines), vertical velocity (thin lines) at s=195m (green), s=327m (blue), s=330m (black), and s=361m (red). Measurement locations are provided in Fig.1.

In Zone 1, the concentration spectra initially show a rapid decrease in energy density as the dye is being mixed both vertically and horizontally (Fig.6, compare green and blue lines). The dominant time scale of the dye motions in this region is O(100 s), shorter than the dominant low-frequency time scales in the fluid motions (Fig.5). This is due to the

Journal of River Engineering
Volume 2, Issue 9, 2014
http://www.scijour.com/jre
SCIJOUR

fact that the dye patch has not reached the scales of the underlying larger fluid motions. In Zone 1 the smaller scale fluid motions play an equal role in the dye mixing resulting in flatter concentration spectra between 0.02 and 0.1 Hz and a high frequency drop-off similar to the ADV spectra. As the mixing proceeds from predominantly 3D to 2D, a reduction in overall concentration energy density is observed and low-frequency motions become dominant, consistent with the ADV velocity spectra (compare blue and black lines in Fig.5). The high frequency drop-off is significantly weaker than observed in the velocity spectra showing that small-scale dye variability is decoupling from the corresponding fluid motions. The low-frequency dominance persists as the dye reaches the end of the stream and the high frequency variance is now fully uncoupled from the fluid motion resulting in white noise (red lines in Fig.6).

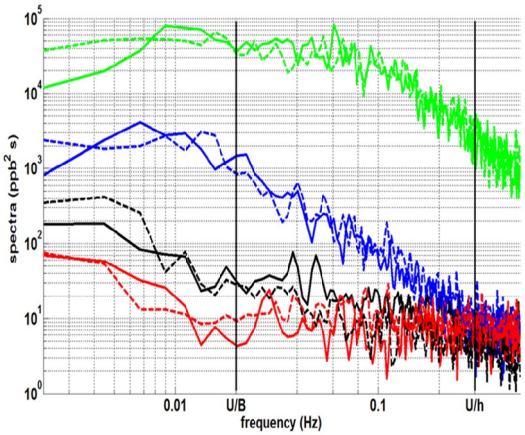

Fig.6. Surface dye concentration spectra observed at s=28 m (green), s= 110 m (blue), s = 313 m (black) and s = 550m (red) for releases T1 (solid) and T2 (dashed). Measurement locations are provided in Fig.1.

MODELING

The 3D mean and turbulent flow fields and consequent transport and mixing are investigated using the numerical model Delft3D-FLOW, which solves the RANS equations for the horizontal motion, continuity, and transport under the incompressible fluid, shallow water and Boussinesq assumptions. Delft3D is a highly adaptable open source modeling suite, which has been used for a wide range of applications with a range from large length and time scales (1000 km, 100 years) to small scale modeling such as this study (10 m, 1 s).

Small-scale motions, not resolved by the model grid, are related to flow quantities by a choice of vertical turbulence closure models. A *k-ε* turbulence closure method is chosen to calculate the isotropic 3D component of eddy viscosity, υ_{3D}. However, turbulence is anisotropic for natural river flows, with the horizontal eddy viscosity coefficient, υ_H, being larger than the vertical eddy viscosity, υ_V. To account for anisotropy, an additional horizontal viscosity component is added due to sub-grid scale horizontalturbulence, υ_{SGS}. Sub-grid scale turbulence is estimated with a Horizontal Large Eddy Simulation (HLES) approximation, which uses a high-pass filter operation to account for energy lost due to grid scale dependent numerical dissipation and truncation [21]. User prescribed HLES parameter inputs for all simulations are: slope in log-log spectrum (-5/3), dimensional number (3), Schmidt number, σ_c, which is the ratio of momentum diffusivity and mass diffusivity(0.7), spatial low-pass filter coefficient (0.333), and relaxation time (0.5 min). Delft3D-FLOW also allows for user specified vertical, υ_V^{back} and horizontal, υ_H^{back} background viscosity terms to account for turbulent motions not captured in the overall execution of the model simulation. The vertical viscosity is then given by:

$$\upsilon_V = \upsilon_{mol} + \max\left(\upsilon_V^{back}, \upsilon_{3D}\right), \quad (5)$$

Where υ_{mol} is molecular diffusion, which is 10^{-6} m^2/s for water. The horizontal viscosity is a superposition of all three terms given by:

$$\upsilon_H = \upsilon_H^{back} + \upsilon_{3D} + \upsilon_{SGS}. \quad (6)$$

The 3D advection/diffusion equation provides the basis to describe the transport of dye, *C*, downstream from a discharge source, *S;*

$$\frac{\partial c}{\partial t} + u_s\frac{\partial c}{\partial s} + u_n\frac{\partial c}{\partial n} + u_z\frac{\partial c}{\partial z} = \frac{\partial}{\partial s}\left(D_H\frac{\partial c}{\partial s}\right) + \frac{\partial}{\partial n}\left(D_H\frac{\partial c}{\partial n}\right) + \frac{\partial}{\partial z}\left(D_V\frac{\partial c}{\partial z}\right) - \lambda + S \quad (7)$$

whereD_V and D_H are the vertical and horizontal turbulent diffusion coefficients, defined as, $D_V = \upsilon_V/\sigma_c$, $D_H = \upsilon_H/\sigma_c$ where $\sigma_c$is the Prandtl-Schmidt number and (5) and (6) are used. For a perfectly passive concentration, $\sigma_c$is one, however, previous 3D numerical model research has shown that using $\sigma_c$less than one provided better results for compensating for anisotropic turbulence structure [22]. Delft3D-FLOW formulates $\sigma_c$as a function of stratification. However, there are no density differences in this study, and $\sigma_c$is kept constant at 0.7. λ can be prescribed to model a first order non-conservative decay process, but since the concentration is conserved λ=0.

To maintain numerical stability and maximize time step, Delft3D-FLOW uses an Alternating Direction Implicit (ADI) method that splits one time-step, Δt, into two stages [23-25]. Each stage consists of half Δt where all the terms of the model equations are solved with second order accuracy in space. The size of Δt is constrained by grid resolution based on the Courant number, CFL, for wave propagation:

$$CFL = 2\Delta t\sqrt{gh\left(\frac{1}{\Delta s^2} + \frac{1}{\Delta n^2}\right)} < 4\sqrt{2}, \quad (8)$$

whereΔs, Δn, are the grid spacing in the streamwise and transverse directions.

The model domain for simulating the field measurement channel consists of 500 2-m grid cells in the stream wise direction, 100 1-m grids cells in the transverse direction. Model bathymetry is created from the measured bathymetry using the triangular interpolation method. The impermeability of the bed is prescribed by a zero flux at the bottom. Constant water elevation boundary conditions obtained from GPS-survey measurements of water elevation are specified at the upstream and downstream open boundaries. Bottom roughness ($z_0 = k_s/30$) is based on the Nikuradse roughness length,k_s. A value of k_s =40mm (D50), which is equal to the measured median grain size, provided the most accurate simulation results. Vertical mixing is

Journal of River Engineering
Volume 2, Issue 9, 2014
http://www.scijour.com/jre
SCIJOUR

important. Therefore, only 3D simulations are used in this study. A continuous surface passive concentration release is simulated in the model domain from the same position as the field experiment. Model calculations are performed with a time step of 0.3 s satisfying the accuracy condition given by Eq.8. (using a smaller time step of 0.03 s gave similar results). Adding vertical and/or horizontal background viscosity, Eq. 5 and 6, did not improve model accuracy and were subsequently omitted. With these settings the model accuracy, R^2, for the mean flow speed is 0.87, for the water elevation is 0.97 and for the dye concentration prediction is 0.86. Predicted and observed dispersion calculated with Eq. 4 for both model and observations show a close correspondence throughout the model domain (Fig.3). The mismatch in zones 3 and 4 for test T1 are due to incomplete transverse sampling discussed in the Channel Flow Features section. Based on the above sensitivity analysis, all subsequent model simulations discussed below use the settings above with sub-grid-scale viscosity obtained from the HLES approximation, and no background viscosity.

DISCUSSION

Channel features straight (IS), constriction (IC), riffle (IR) and embayment (IE)) are isolated and idealized in five separate numerical simulations to assess their relative and combined importance on channel mixing. Idealized bathymetries are based on the natural channel geometry and their location is based on a distance from the concentration source (Fig.7). All bathymetries are constructed by modifying a straight channel 23 m wide with a centerline depth of 1.6 m and a transverse depth profile based on a straight channel (Fig.7a). IC and IR span 70 m and are located in Zone 3rc. The IC case narrows the channel by 66% to its narrowest of 8 m between 197<s<243m. The IR case is a shallow, 0.5 m, section located 205<s<235 m. The IE case is a widening of the channel by 7m on river-right bank at Zone 3e that spans 110m, 240<s<350 m.

Transverse Dispersion Comparisons

The mixing in all idealized channels behave similarly to the IS case within Zone 1 and 2, in which the plumes are undisturbed and centered in their respective channels, dispersion increase is small and linear (k_n=0.005 m^2/s) (Fig.8 and Fig.9). Entering Zone 3rc, IC bathymetric features causes a noticeable contraction (Fig.8b), reflected by a decrease in dispersion (Fig.9 cyan), whereas IR bathymetric feature causes an expansion, as the channel shallows (Fig.8c), resulting in an increased dispersion (Fig.9 red). Between Zones 3rc and 3e, the IR plume is contracted and sharp concentration gradients develop. Clean water present along the mixing interface indicates the presence of recirculating eddies on the channel banks. The corresponding concentration patterns suggest these eddies are drawing concentration out of the jet core and transporting it laterally and upstream along channel banks resulting in a rapid increase in dispersion (k_n =0.25 m^2/s). IC and IE bathymetric features also cause a rapid increase in dispersion (k_n =0.17 m^2/s, 0.07 m^2/s for IC and IE respectively) (Fig.9 cyan and green). IC concentration patterns indicate similar, though less effective, recirculating eddies on the channel banks. IE concentration patterns do not exhibit mixing due to eddies, however, the plume is drawn towards the embayment, briefly increasing dispersion (Fig.9), before the downstream end of the embayment feature contracts and centers the plume (Fig.8d). IR results in the highest dispersion, which is 3 times larger than the IS dispersion at s=450m. IC dispersion is 2 times larger than the IS dispersion. Surprisingly, the excursion of the IE plume into the embayment has little influence on overall dispersion resulting in the smallest dispersion, which is only 10% greater than the IS dispersion (Fig.9). Within Zone 4 for all cases, plumes are symmetrical and centered in the channel. Here k_n is similar to the IS case (Fig.8 and Fig.9).

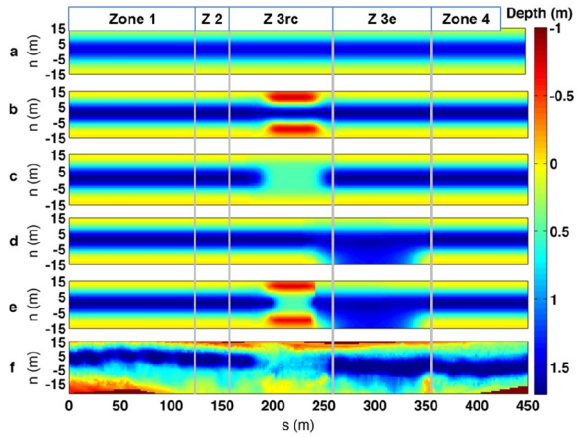

Fig.7. Idealized bathymetry for a) straight channel (IS), b) constriction (IC), c) riffle (IR), d) embayment (IE), e) combined (CP) and f) actual bathymetry. Depth scale colorscale (m) located on the right.

The concentration spreading of the isolated features is compared with the idealized combined bathymetry (CP), composed of all idealized channel features (Fig.8e and Fig.9 (magenta)). Spatially large velocity structures (e.g. vortex shedding) are present in the CP (Fig.8e) that are not present in the isolated cases. When the isolated IE case, which had little effect on mixing, is combined with IR and IC bathymetry, a large eddy is formed within the embayment that greatly enhances mixing (Fig.8e and Fig.9 (magenta)). The CP embayment eddy spans ~75 m in the streamwise direction and occupies ~18m (60%) of the channel width. Additionally, vortex pairs are present on river-left with one eddy near Zone 3rc exit, which contracts the plume and forms sharp concentration gradients, and another larger eddy, which protrudes into the thalweg causing the jet to meander sharply. The effect of these combined velocity structures enhance mixing as dye is drawn from the jet core toward the banks (Fig.8e).

CP dispersion is compared with the total dispersion from the linear superposition of all individual feature dispersions (Fig.9 black). Though there are similarities between CP and the superposition dispersion pattern, such as initial slow linear spread follow by a rapid spreading, there are significant differences between them, which highlight the non-linear effect of combined channel geometries. The CP spreading rate is a factor of 3 greater than superposition

Journal of River Engineering
Volume 2, Issue 9, 2014
http://www.scijour.com/jre
SCIJOUR

(CP: k_n=2.0 m^2/s, summation: k_n=0.64 m^2/s) and the maximum dispersion is a factor of 2 greater (Fig.9). At *s*=450 m the CP dispersion has achieved complete transverse mixing where σ^2_n is a constant 35 m^2(Fig.8e and Fig.9 magenta). Extrapolated distances of complete mixing for isolated cases, assuming constant mixing without additional bathymetric features, range between 1000 and 2000 m, for IR and IS respectively.

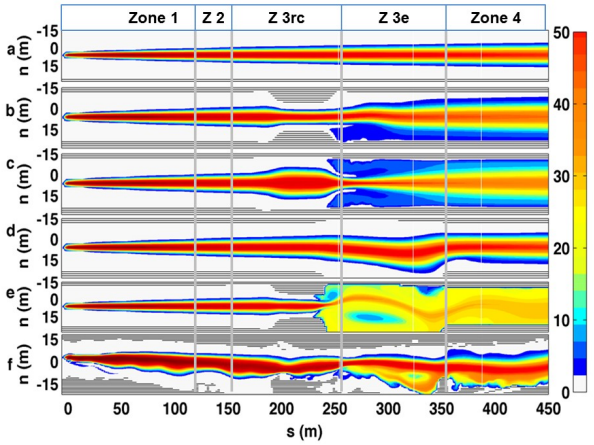

Fig.8. Modeled surface concentrations in ppb for a) straight channel (IS), b) constriction (IC), c) riffle (IR), d) embayment (IE), e) combined (CP) and f) actual bathymetry. Concentration scale colorscale (ppb) located on the right.

Spatial concentration patterns between the natural bathymetry and the synthetic CP bathymetry are comparable (Fig.8e and f), but differences are observed. The natural system has more inherent bathymetric and shoreline variability, which cause more spreading in Zones 1 and 2 (Fig.9). Note that the natural simulation includes an upstream riffle, which was not included in the idealized cases. The boundary condition for the idealized channel was steady state. In the natural simulation upstream bathymetry features introduce initial unsteady velocities equal to 0.5 m/s leading to higher mixing in Zones 1-2. In Zone 3, geometric controls confine both CP and natural plumes. Similar to the IR and CP cases, the natural plume is contracted by recirculating eddies on the channel banks at the exit of Zone 3rc. Due to channel geometry these eddies are smaller in the natural setting but their role in enhancing mixing within the embayment is similar. The CP has an active eddy formation on the river-left at *s*=320 m and *s*=350 m, discussed above, whereas the natural system does not. The concentration mixing on river-left observed in the CP case is not present in the natural case. On river-right an embayment eddy is present but it is more elongated, with its center ~50 m farther downstream than the CP case (Fig.8f). In Zone 4 there is a second separation eddy formed in the lee of the large bank protrusion at *s*=350 m, drawing concentration towards river-right. The combination of weak, to no, eddy activity on river-left and strong separation eddies formed by the large bank irregularities on river -right are responsible for the pronounced skewness in modeled concentrations (Fig.8f) and in situ concentration transects (Table.1). An important difference in the natural case are that large bank irregularities produce smaller "secondary" circulation eddies, which are not in contact with the main stream. An example of one such secondary eddy can be seen at *s*~310 m on river-right. This eddy is rotating counter-clockwise and clearly drawing some dye concentration into it (Fig.8f). Experiments on entrainment in groins fields, which are geometrically similar to the natural embayment feature, have shown eddies within groins develop similar primary and secondary circulation structures. These structures have been shown to control the mixing by trapping concentration within “dead zones” and lagging release to the main stream [26]. It is hypothesized that the natural embayment will trap dye and thereby slowdown the release into the main channel in the same way.

These cases demonstrate that small differences in bathymetry result in significant differences in mixing behavior. Therefore, numerical modeling is required to accurately predict non-linear effects in natural mixing.

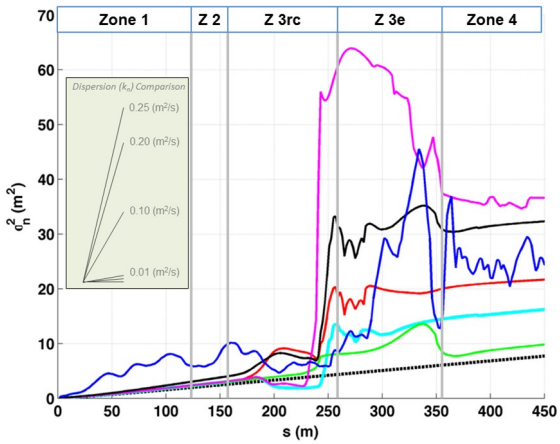

Fig.9. Dye concentration dispersion for a straight channel, IS (black dashed), constriction, IC (cyan), riffle, IR (red), embayment, IE (green), combined, CP (magenta), summation (black) and actual channel bathymetry (blue). The riffle and the constriction produce a jet-like flow that yields the most individual feature spreading. The embayment yields a small increase in mixing over the straight case. The differences between the summation (black) and combined (magenta) exemplify the non-linear mixing response.

DOMINANT PROCESSES

Simulations confirm channel features can dominate transport and mixing. Small differences in the location and degree of bathymetry irregularity significantly modify mixing. Concentration patterns and corresponding dispersion statistics cannot explain the causal physical processes. In this section, the roles of the underlying forcing mechanisms are investigated. The effects of mean flow, vertical shear, and turbulence on transport and mixing are examined separately using the depth-averaged momentum flux equation in the stream-wise direction

$$\frac{\partial(h\overline{u_s}^2)}{\partial s}+\frac{\partial(h\overline{u_s}\overline{u_n})}{\partial n}-\frac{\partial(hT_{sn})}{\partial n}+\frac{\partial(hT_{ss})}{\partial s}=-gh\frac{\partial\overline{\eta}}{\partial s}-c_f\left(\sqrt{\overline{u_s}^2+\overline{u_n}^2}\right)^2 \quad (9)$$

(1) (2) (3) (4) (5) (6)

This equation quantifies the components of the lateral momentum flux gradients (Eq. 9, terms 2 and 3) along the

Journal of River Engineering
Volume 2, Issue 9, 2014
http://www.scijour.com/jre
SCIJOUR

CP channel, where $\overline{u_s}$ and $\overline{u_n}$ are the time and depth-averaged streamwise and transverse velocities, $\bar{\eta}$ is the water elevation, g is gravitational acceleration, $T_{sn}$is the sum of the depth-averaged transverse momentum fluxes due to vertical shear and turbulence, $T_{ss}$is the sum of depth-averaged streamwise momentum flux and $c_f$is a quadratic-law friction coefficient [27]. T_{sn}expressed in the kinematic form is,

$$T_{sn} = -\langle(u_{sz} - \overline{u_s})(u_{nz} - \overline{u_n})\rangle - \langle u'_{sz}u'_{nz}\rangle \quad (10)$$

where$u_{sz} - \overline{u_s}$ and $u_{nz} - \overline{u_n}$ are measures of time-averaged vertical shear. u_{sz}, u_{nz}, are the local time-averaged streamwise and transverse velocities at each vertical level, and u'_{sz} and u'_{nz} are the velocity fluctuations at each vertical level where $\langle\ \ \rangle$ indicates ensemble time-averaging.

It is assumed that the dye acts as a quasi-passive tracer and follows the flow of the water. The lateral momentum components can be thought of as two processes; 1) the lateral transport of the concentration following, $\overline{u_s u_n}$ flowing along the mean stream lines, and 2) the plume is mixed by mean vertical shear advected laterally $\langle(u_{sz} - \overline{u_s})(u_{nz} - \overline{u_n})\rangle$ and turbulence $\langle u'_{sz}u'_{nz}\rangle$. The transverse gradients of these terms provide the depth-averaged convective acceleration contribution for each process. CP momentum flux patterns shown in (Fig.10) highlight the dominance of the mean flow and the magnitude of geometry induced accelerations. Positive momentum flux values (Fig.10b, red colors) indicate acceleration toward river-left and negative momentum flux values (Fig.10b, blue colors) indicate acceleration toward river-right. In straight sections, all lateral momentum gradients are relatively small with the transverse gradients of $\overline{u_s u_n}$being the largest by two orders of magnitude, < 0.01 cm/s^2(Fig.10, line plot at s=160 m). Near channel features, the transverse $\overline{u_s u_n}$ gradients of O(10 cm/s^2) remains dominant and all component accelerations are two to three orders of magnitude larger than within the straight sections. Zone 3rc accelerations force water inward and a narrow jet core is centered in the channel (Fig.10b, near zero momentum flux strip). Exiting Zone 3rc, large strips of positive and negative acceleration indicate an organized converging jet oriented towards river-left (Fig.10b and line plot at s=251 m). The jet turns at s=275 m towards river-right and begins to broaden at a slower rate, indicated by the reversed accelerations (Fig.10b and line plot at s=321m). After the turn, the accelerations are reduced by half and in opposite direction. At the end of the embayment the jet turns again and is forced back towards the center, flow is weakly convergent (Fig.10b and line plot at s=385). On river-left and river-right, the counter rotating vortexes are visible with large areas of stagnant water, highlighting possible concentration trapping regions.

CONCLUSION

A process based study of transport and mixing was conducted in a channel of the Kootenai River, Idaho. The 550m channel reach contains a constriction, riffle and large bank irregularities with a natural embayment. River conditions were stationary, discharge was constant, and there was no rain during the experiment. These conditions resulted in quasi-steady state concentration profiles. The study entailed two 1-hour continuous concentration releases in a straight 1.6 m deep reach. A combination of stationary and moving-platform observation techniques were used to obtain comprehensive measures of velocity and dye concentration throughout the study reach. Under the assumption of stationarity, 47 velocity profiles were measured at various locations throughout the reach using 5 acoustic Doppler current profilers, and 3D turbulence was measured at 5 locations using an acoustic Doppler velocimeter mounted on a moveable frame. Ten fluorescent dye concentration sensors were used to continuously measure profiles at 3 locations and at the surface at the source and near the end of the reach during the dye experiments. The surface dye concentration field was measured spatially throughout the 550m reach using 3, 1-m, moveable catamarans equipped with collocated fluorescent dye concentration and GPS sensors. Additionally, velocity, discharge, bathymetry and water level surveys were conducted.

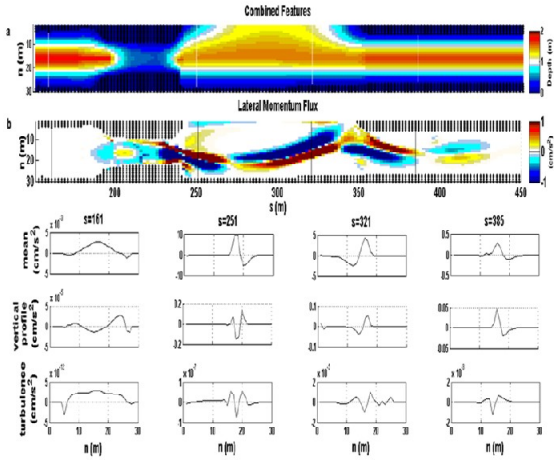

Fig.10. a) Bathymetry of simulated combined features with depth color scale located on the right, b) Colormap of the lateral momentum flux estimated by Eq. 10 with color scale located on the right. Four transects of each lateral momentum flux term: c) $\frac{\partial \overline{u}_s \overline{u}_n}{\partial n}$, d) $\frac{\partial \overline{(u_{sz} - \overline{u}_s)(u_{nz} - \overline{u}_n)}}{\partial n}$ and e) $\frac{\partial \overline{(u_{sz}{}' u_{nz}{}')}}{\partial n}$ for s=161 m, s=251 m, s=321 m, and s=385 m.

Lateral dispersion was quantified using integrated transverse concentration profiles as measured by calculating the 2nd moment of transverse concentration profiles at 136 locations along the channel during the two experiments. Measurement and dispersion estimates show that natural channel mixing is highly variable and predominantly controlled by channel features. The sampling during the second experiment did not extend across the entire channel at all locations, resulting in underestimating σ_n^2 values. However, the two experiments gave similar spreading values and spatial behavior after normalizing by the variance of a uniform distribution over the respective sampled width, which means the experiments are repeatable at least in the mean value of σ_n^2 and verifies the assumption that the forcing was stationary. Lateral diffusion coefficients were estimated from the dispersion gradients with mean values ranging 0.01-0.06 m^2/s, which are comparable to values found by other authors in natural rivers (Rutherford

1994). The streamwise envelope of the dye concentration distribution initially decayed as C_{max}~$s^{-3/2}$, over the first 100m indicative of 3D mixing behavior in the near field. After 100m the dye was mixed over the vertical and decayed as C_{max}~s^{-1}, which describes 2D mixing behavior.

The concentration and velocity spectra confirm k_n is highly variable in the vicinity of channel irregularities. Velocity is isotropic at f >~0.3 Hz which scales with mean velocity divided by depth [20]. For f >0.3 Hz, the flow is anisotropic and there are significant differences in the transverse velocity components at different streamwise locations. ADV spectra downstream of the bathymetry features, Zone 3, contain one order of magnitude more transverse energy in the lower frequencies than ADV spectra upstream, Zone 2, and downstream, Zone 4. This spectral frequency band is delineated by dimensional scaling mean velocity divided by river width at f~0.02 Hz. The concentration spectra initially show equal roles of diffusive and large scale motion in the dye mixing. However, as the dye is mixed vertically, the 2D behavior exhibits a dominance of the low-frequency motions and a weaker high frequency drop-off that indicates the small-scale dye variability becomes decoupled from the higher frequency fluid motions. The low-frequency dominance of the velocity spectra in the concentration spectra indicates that the dye is mixed coherent velocity structures play a larger role in mixing than the underlying turbulence.

Dispersion cannot be estimated by individually parameterizing and linearly adding the effects of isolated channel features. Through numerical modeling, the impact of the prominent channel features on mixing is quantified, and the mechanisms of transverse dispersion examined. First, the open source, 3D numerical model, Delft3D-Flow, was initialized and validated against the field observations. The numerical model produced good agreement with measurements of velocity (R^2=0.87), water elevation (R^2=0.97), as well as transport and mixing (R^2=0.86). To examine the mixing processes, the prominent bathymetric features of a constriction, riffle and embayment were isolated and idealized. The model was used to calculate transverse dispersion for idealized bathymetry for the isolated prominent features of the constriction, riffle and embayment, a combined idealized bathymetry and the actual bathymetry. It was found that linearly summing the dispersion for each of the isolated prominent features greatly underestimated the dispersion of the combined idealized bathymetry and the actual bathymetry.

The non-linear mixing of passive tracer dye was examined by the calculating the effects of the mean flow, vertical shear and turbulence using the depth-averaged momentum flux equations in the transverse direction. In the near field <100 m from release point, natural river modeling requires resolution of larger scale velocity structures and small scale diffusive processes. However, beyond the near field, as the concentration plume is mixed fully in the vertical, the behavior becomes 2D, and the large-scale coherent velocity structures controlled by bathymetry features dominate concentration plume spreading. These investigations indicate that coherent velocity structures controlled by bathymetric variability at all scales are responsible for the spatial concentration distribution, restricting lateral transport and trapping material, resulting in a strongly non-linear mixing response.

Acknowledgements: We extend our appreciation to the many personnel who assisted in obtaining the river data set: Jenna Brown, Keith Wyckoff , Ron Cowen, Patrick Rynne, Will Ashley and Christopher Tuggle. We appreciate the logistical support from the Kootenai Tribe of Idaho and U.S. Geological Survey, particular Gary Barton and Jon Nelson.

REFERENCES

[1] ***Demuren, A. O., and Rodi, W.,*** *Calculation of flow and pollutant dispersion in meandering channels:, v. 172, 1986, p. 63-92.*

[2] ***Simoes, F. J. M., and Wang, S. S. Y.,*** *Numerical prediction of three-dimensional mixing in a compound open channel: Journal of Hydraulic Research, v. 35, 1997, p. 619-642.*

[3] ***Gualtieri, C.****, RANS-based simulation of transverse turbulent mixing in a 2D geometry: Environmental Fluid Mechanics, v. 10, 2010, p. 137-156.*

[4] ***Wilson, C., Boxall, J. B., Guymer, I., and Olsen, N. R. B.****, Validation of a three-dimensional numerical code in the simulation of pseudo-natural meandering flows: Journal of Hydraulic Engineering-ASCE, v. 129, 2003, p. 758-768.*

[5] ***Wilson, C., Guymer, I., Boxall, J. B., and Olsen, N. R. B.****, Three-dimensional numerical simulation of solute transport in a meandering self-formed river channel: Journal of Hydraulic Research, v. 45, 2007, p. 610-616.*

[6] ***Rutherford, J.C.****, River Mixing: Wiley, New York 1994.*

[7] ***Dow, K. E., Steffler, P. M., and Zhu, D. Z.****, Case Study: Intermediate Field Mixing for a Bank Discharge in a Natural River: Journal of Hydraulic Engineering-ASCE, v. 135, 2009, p. 1-12.*

[8] ***Fischer, H.B., List, E.J., Koh, R.C.Y., Imberger, J, and Brooks, N.H.****, Mixing in inland and coastal Waters: New York: Academic Press, 1979.*

[9] ***Constantinescu, G., Sukhodolov, A., and McCoy, A.****, Mass exchange in a shallow channel flow with a series of groynes: LES study and comparison with laboratory and field experiments: Environmental Fluid Mechanics, v. 9, 2009, p. 587-615.*

[10] ***Barton, G.J., Moran, E.H., and Berenbrock, Charles****, Surveying cross sections of theKootenai River between Libby Dam, Montana, and Kootenay Lake, British Columbia, Canada: U.S. Geological Survey Open-File Report, 2004, 1045-1080.*

[11] ***Barton, G.J., McDonald, R.R., Nelson, J.M., and Dinehart, R.L.****, Simulation of flowand sediment mobility using a multidimensional flow model for the white sturgeon critical-habitat reach, Kootenai River near Bonners Ferry, Idaho: U.S. Geological Survey Scientific Investigations Report 5230-5284.*

[12] ***Fosness, R.L., and Williams, M.L.****, Sediment characteristics and transport in the Kootenai River white sturgeon critical habitat near Bonners Ferry, Idaho: U.S. Geological Survey Scientific-Investigations Report 2009, 5228-5268.*

[13] ***Legleiter, C. J., and Kyriakidis, P. C.***, *Forward and inverse transformations between cartesian and channel-fitted coordinate systems for meandering rivers: Mathematical Geology, v. 38, 2006, p. 927-958.*

[14] ***Brown, J., C. Tuggle, J. MacMahan, A. Reniers***, *The use of autonomous vehicles for spatially measuring mean velocity profiles in rivers and estuaries, Intelligent Service Robotics. 2011, doi: 10.1007/s11370-011-0095-6*

[15] ***Bright Concentrations Division***, *Technical Data Bulletin, 2002.*

[16] ***MacMahan, J., Brown, J., and Thornton, E.***, *Low-Cost Handheld Global Positioning System for Measuring Surf-Zone Currents: Journal of Coastal Research, v. 25, 2009, p. 744-754.*

[17] ***Geyer, W. R., Chant, R., and Houghton, R.***, *Tidal and spring-neap variations in horizontal dispersion in a partially mixed estuary: Journal of Geophysical Research-Oceans, v. 113, 2008.*

[18] ***Clark, D. B., Feddersen, F., and Guza, R. T.***, *Cross-shore surfzone concentration dispersion in an alongshore current: Journal of Geophysical Research-Oceans, v. 115, 2010.*

[19] ***Fischer, H.B.***, *Longitudinal dispersion and turbulent mixing in open channel flow, Ann. Rev. Fluid Mech., 5, 1973, 59-78*

[20] ***Sukhodolov, A. N., and Uijttewaal, W. S. J.***, *Assessment of a River Reach for Environmental Fluid Dynamics Studies: Journal of Hydraulic Engineering-ASCE, v. 136, 2010, p. 880-888.*

[21] ***Uittenbogaard, R.E.,*** *Model for eddy diffusivity and viscosity related to sub-grid velocity and bed topography. Note, WL | Delft Hydraulics, 1998.*

[22] ***Demuren, A. O., and Rodi, W.,*** *Calculation of turbulence-driven secondary motion in non-circular ducts: Journal of Fluid Mechanics, v. 140, 1984, p. 189-222.*

[23] ***Leendertse, J.J.***, *Aspects of a computational model for long-period water-wave propagation. Ph. D. Thesis, RM-5294-RR, Rand Corporation, Santa Monica, 1967.*

[24] ***Leendertse, J.J. and E.C. Gritton***, *A water quality simulation model for well mixed estuaries and coastal seas: Vol. II, Computation Procedures, Report R-708-NYC, The Rand Corporation (Santa Monica), 1971.*

[25] ***Leendertse, J.J., R.C. Alexander and S-K. Liu***, *A three-dimensional model for estuaries and coastal seas, The Rand Corporation (Santa Monica) 1973.*

[26] ***Weitbrecht, V., Socolofsky, S. A., and Jirka, G. H.***, *Experiments on mass exchange between groin fields and main stream in rivers: Journal of Hydraulic Engineering-ASCE, v. 134, 2008, p. 173-183.*

[27] ***Rhoads, B. L., and Sukhodolov, A. N.***, *Lateral momentum flux and the spatial evolution of flow within a confluence mixing interface: Water Resources Research, v. 44, 2008.*